© 2015. Published by The Company of Biologists Ltd | Development (2015) 142, 2048-2057 doi:10.1242/dev.119602

RESEARCH ARTICLE

Compensatory branching morphogenesis of stalk cells in the *Drosophila* trachea

Deanne Francis and Amin S. Ghabrial*

ABSTRACT

Tubes are essential for nutrient transport and gas exchange in multicellular eukaryotes, but how connections between different tube types are maintained over time is unknown. In the *Drosophila* tracheal system, mutations in *oak gall* (*okg*) and *conjoined* (*cnj*) confer identical defects, including late onset blockage near the terminal cell-stalk cell junction and the ectopic extension of autocellular, seamed tubes into the terminal cell. We determined that *okg* and *cnj* encode the E and G subunits of the vacuolar ATPase (vATPase) and showed that both the V0 and V1 domains are required for terminal cell morphogenesis. Remarkably, the ectopic seamed tubes running along vATPase-deficient terminal cells belonged to the neighboring stalk cells. All vATPase-deficient tracheal cells had reduced apical domains and terminal cells displayed mislocalized apical proteins. Consistent with recent reports that the mTOR and vATPase pathways intersect, we found that mTOR pathway mutants phenocopied *okg* and *cnj*. Furthermore, terminal cells depleted for the apical determinants Par6 or aPKC had identical ectopic seamed tube defects. We thus identify a novel mechanism of compensatory branching in which stalk cells extend autocellular tubes into neighboring terminal cells with undersized apical domains. This compensatory branching also occurs in response to injury, with damaged terminal cells being rapidly invaded by their stalk cell neighbor.

KEY WORDS: Tubulogenesis, *Drosophila*, vATPase, Tor, Apical polarity

INTRODUCTION

Tubular networks are essential for nutrient transport, enzyme secretion and ion homeostasis (Andrew and Ewald, 2010; Strilić et al., 2010). In many cases, organs are composed of distinct tube types, including multicellular, autocellular or seamless tubes (Andrew and Ewald, 2010). In the vascular system, for example, multicellular capillaries connect via seamless tubes (Blum et al., 2008; Herwig et al., 2011; Wolff and Bär, 1972). Likewise, the *Drosophila* tracheal system is composed of interconnected tubes of different types (Fig. 1A,B) (Ghabrial et al., 2003; Samakovlis et al., 1996). Prior work (Song et al., 2013) suggested that connections between tubes of different architectures requires ongoing maintenance, but the maintenance program is not well understood. Here we characterize mutants with late onset connection defects and uncover an unappreciated ability of autocellular seamed tubes to undergo compensatory growth and branching when terminal cells are unable to expand their apical membrane domain.

Department of Cell and Developmental Biology, University of Pennsylvania Perelman School of Medicine, Philadelphia, PA 19104, USA.

*Author for correspondence (ghabrial@mail.med.upenn.edu)

Received 7 November 2014; Accepted 16 April 2015

During fly development, ten pairs of epithelial sacs remodel into a tubular tracheal network in which large multicellular tubes connect to finer autocellular tubes, which in turn connect to intracellular seamless tubes that mediate gas exchange (Fig. 1A,B). Tracheal cells are epithelial, with their apical domain facing the tube lumen (Isaac and Andrew, 1996; Wodarz et al., 1995). Tip cells, located at the ends of primary branches, guide tube outgrowth and later differentiate into fusion cells or terminal cells and form intracellular seamless tubes. Long terminal cell seamless tubes branch extensively, whereas fusion cell tubes are short and unbranched. In dorsal branches, two tip cells connect to a Y-shaped stalk cell. This Y-shaped autocellular tube is bifurcated at the distal end to make independent connections to each tip cell (Samakovlis et al., 1996) (Fig. 1B). The interface between the stalk cell and terminal cell is simple, whereas the connection to the fusion cell is more complex: the stalk cell extends its seamed tube into the fusion cell, like “a finger poking into a balloon” (Gervais et al., 2012; Uv, 2003), such that stalk cell apical membrane surrounds almost the entire fusion cell lumen (Gervais et al., 2012). How the stalk cell makes and maintains these different connections, and what genetically and molecularly distinguishes them, remains undetermined.

To better understand seamed-to-seamless tube connections, we characterized mutations in *oak gall* (*okg*) and *conjoined* (*cnj*), which confer identical tube connection defects (Ghabrial et al., 2011). Sequence analysis revealed that *okg* and *cnj* carry mutations in *Vha26* and *Vha13*, which encode the E and G subunits of the vacuolar ATPase (vATPase). Terminal cells deficient for vATPase showed defects in apical polarity and apical membrane domain size, and neighboring stalk cells extended seamed tubes into them. Depletion of the apical determinants atypical Protein kinase C (aPKC) or Par-6 reproduced key features of vATPase-deficient terminal cells. This implied that wild-type stalk cells compensate for neighboring terminal cells with undersized apical domains by extending branched autocellular tubes into the terminal cell lumen and displacing the terminal cell apical membrane distally. Compensatory stalk cell branching also occurs upon physiological challenge, not just in genetically compromised animals: we find that injured terminal cells are rapidly invaded by their neighboring stalk cell.

RESULTS

Ectopic branched autocellular tubes extend into *okg* and *cnj* terminal cells

We characterized the role of *okg* and *cnj* (Ghabrial et al., 2011) in tube architecture and connectivity in mosaic animals, with a focus on the connection between autocellular and seamless tubes. In wild-type larvae, a gas-filled autocellular tube connects the stalk cell to its terminal cell neighbor. Within the terminal cell, the seamless tube branches extensively (Fig. 1B,C). Cells mutant for *okg* or *cnj* exhibited identical tracheal defects. Mutant terminal cells showed a

Development (2015) 142, 2048-2057 doi:10.1242/dev.119602

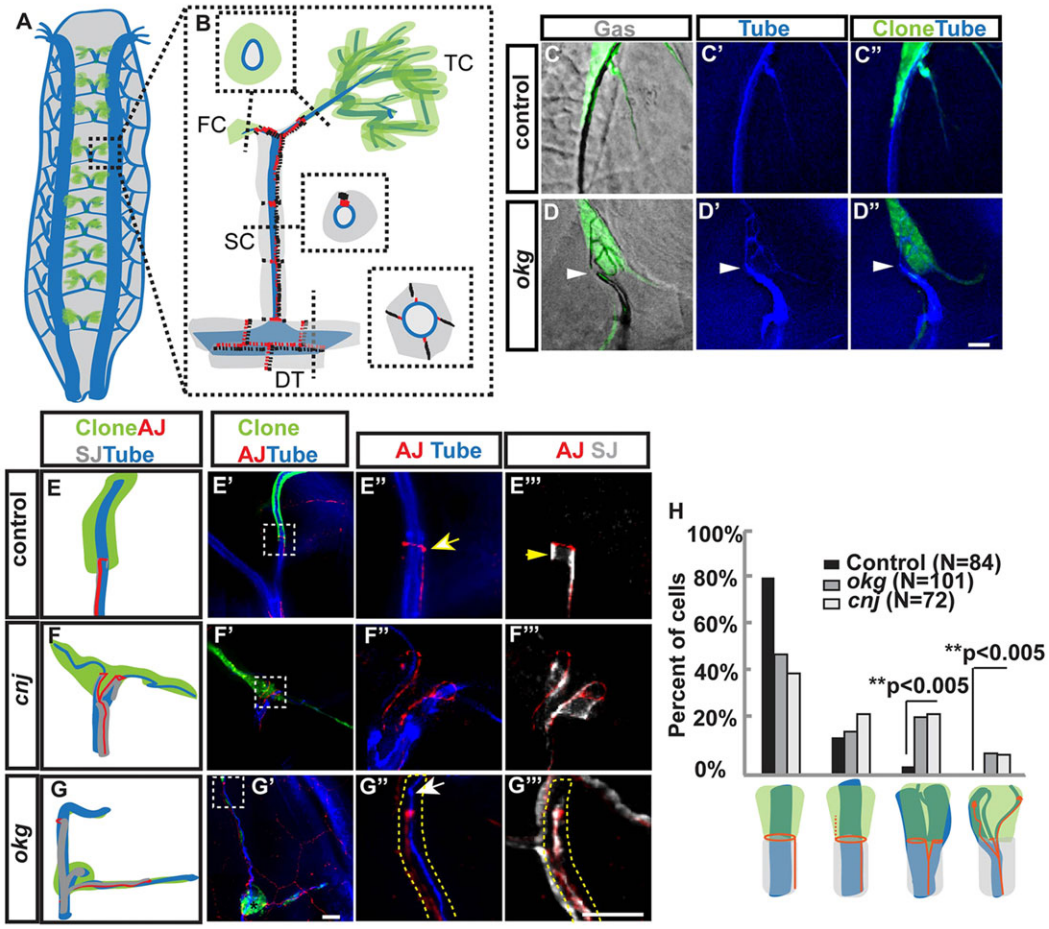

Fig. 1. Autocellular adherens junctions extend into *okg* and *cnj* terminal cells. (A) Schematic of the *Drosophila* third instar tracheal system (tube, blue); dorsal view, anterior top. Dorsal branch terminal cells are indicated (green). (B) Cellular architectures of dorsal branch (TC, terminal cell; FC, fusion cell; SC, stalk cell) and dorsal trunk (DT) tubes are illustrated. Adherens junctions (AJs, red) and septate junctions (SJs, black) are indicated. (C-D″) The terminal cell-stalk cell interface of mosaic third instar larvae, showing positively marked terminal cell clones (*btl*>GFP, green), gas filling (bright field) and tubes (UV, blue). (C) Control terminal cell clone with gas-filled tubes. (D) Unmarked stalk cell with gas-filling gap (arrowhead) and tube constriction (D′,D″, arrowhead) adjacent to *okg* terminal cell clone (green). (E-G‴) Schematics of junctions (E,F,G) and micrographs (E′-G‴). Clone marker (GFP, green) labels homozygous cells. AJ (DE-cadherin, red), SJ (Varicose, gray) and tube (UV autofluorescence, blue) are shown. Boxed regions in E′-G′, enlarged in E″-G‴. Intercellular junctions at the terminal cell-stalk cell interface are indicated (AJ, yellow arrow; SJ, yellow arrowhead). (F-F‴) A *cnj* terminal cell with a class 1 defect: bifurcated autocellular stalk cell tube connects to *cnj* terminal cell via two intercellular junctions (F″,F‴). (G-G‴) An *okg* terminal cell with a class 2 defect: autocellular AJ and SJ line branched tubes within the *okg* terminal cell, two of which end in intercellular junction-like rings (G′-G‴); seamless tube extends beyond rings (G″, white arrow). Asterisk, terminal cell nucleus. (H) Phenotype frequency. First column, terminal cell with exclusively seamless tubes; second column, terminal cell with short seamed and long seamless tubes; third column, terminal cell with multiple connections (class 1 defect); fourth column, terminal cell with branched autocellular tubes (class 2 defect). Statistical significance was determined by Fisher's exact probability test. Scale bars: 10 µm.

gas-filling defect at the stalk cell to terminal cell connection (Fig. 1D, arrowhead). Strikingly, most gas-filling gaps were present in heterozygous stalk cell tubes adjacent to *okg* or *cnj* terminal cells (Fig. 1D′,D″, arrowhead). The gas-filling defect was 100% penetrant, but with late onset (appearing only at third larval instar), and was within the stalk cell rather than the terminal cell in 75% of *cnj* (n=24) and 70% of *okg* (n=30) terminal cell clones (Fig. 1D).

Examination of cell junctions within and between stalk cells and terminal cells revealed two classes of novel stalk cell-terminal cell interface defect. Control terminal cells (81%, n=84) had a single intercellular junction with a neighboring stalk cell, consisting of a ring of adherens junctions (AJs) (Fig. 1E″,E‴, arrow) and a broader ring of septate junctions (SJs) (Fig. 1E‴, arrowhead). Terminal cells typically showed an unbranched seamless tube extending from the intercellular junction towards the nucleus (Fig. 1E,E′), distal to which extensive branching of the seamless tube occurred. A fraction of control terminal cells (15%, n=84) had a nucleus-proximal autocellular tube (<4 µm in length; supplementary material Fig. S1A), as previously described for embryonic (Samakovlis et al., 1996) and larval (Song et al., 2013) terminal cells. A comparable fraction of *okg* (18%, n=101) and *cnj* (25%, n=72) terminal cells had similar segments of short unbranched autocellular tube (Fig. 1H; supplementary material Fig. S1B).

In mutants, we identified a first class (class 1) of defects in which stalk cells formed two or more connections to a neighboring terminal cell (Fig. 1F-F‴); this was evident in 24% of *okg* cells (n=101) and 25% of *cnj* cells (n=72), as compared with 4% of control cells (Fig. 1H). This topology has not previously been described for either wild-type or mutant terminal cells. In more severely affected terminal cells [9% (n=101) *okg* and 8% (n=72) *cnj*] we observed class 2 defects in which long, branched seamed tubes extended well beyond the terminal cell nucleus (Fig. 1G,G′,H). Unlike class 1 seamed tubes,

Development (2015) 142, 2048-2057 doi:10.1242/dev.119602

class 2 tubes branched within the terminal cell and appeared to terminate at ring-like intercellular junctions distal to the terminal cell nucleus – phenotypes never observed in wild type (Fig. 1E,H). Beyond the ring-like structures, seamless tubes extended towards the terminal cell tips (Fig. 1G′,G″). We could not detect any evidence of long autocellular tubes within homozygous mutant terminal cells (supplementary material Fig. S1C,D), suggesting that *okg* and *cnj* connection defects arise late.

cnj and *okg* encode two subunits of the vacuolar H$^+$ ATPase

To understand how *cnj* and *okg* influence tube architecture, we mapped the mutations (Fig. 2A,B). Sequence analysis of candidate genes revealed a *Vha13* mutation in *cnj* and a *Vha26* mutation in *okg* (Fig. 2C,D). *Vha13* and *Vha26* encode the G (13 kDa) and E (26 kDa) subunits of vATPase. A *Vha13* transgene rescued *cnj* tracheal defects, confirming gene identity and suggesting that the mutant allele is a loss of function (Fig. 2E-G′). The cnj^{356} allele carries a deletion that creates a frameshift predicted to encode a larger protein, all but 45 residues of which are novel. The okg^{696} allele is likely to be amorphic, with a nonsense mutation encoding a truncated Vha26 protein. Terminal cell-specific knockdown of *Vha26* recapitulated the *okg* phenotype, with a higher incidence of class 2 defects (45%, n=67; Fig. 2H,H′). The severity of the knockdown phenotype suggested a maternal contribution of *okg* mRNA, early zygotic transcription prior to clone induction, or both. In addition, postembryonic knockdown was sufficient to confer the terminal cell defects (supplementary material Fig. S1E), consistent with a maintenance role of the vATPase.

Loss of proton pumping results in ectopic autocellular tubes

Vha13 and Vha26 function as a heterodimer within the V1 domain (Fig. 3A) and regulate vATPase assembly and disassembly (Hildenbrand et al., 2010; Ohira et al., 2006; Okamoto-Terry et al., 2013; Smardon et al., 2002). Mutation of *okg* or *cnj* should compromise V1 and vATPase assembly, but not V0 function (Doherty and Kane, 1993; Tomashek et al., 1997). Since free V0 can bind SNAREs to promote membrane fusion (Bayer et al., 2003; Di Giovanni et al., 2010; Hiesinger et al., 2005; Liegeois, 2006; Strasser et al., 2011), it was important to test whether tracheal defects resulted from loss of vATPase function or gain of V0 membrane fusion activity. Terminal cells depleted for either V0d or c″ (Fig. 3B-D′) exhibited both class 1 and class 2 phenotypes (n=93 and n=42, respectively; see Fig. 3F for quantification); thus, loss of the holoenzyme is the underlying cause of the phenotype.

To test whether holoenzyme assembly [permitting interactions such as Pak binding (Lin et al., 2012)] is sufficient for tubulogenesis or if enzymatic function (acidification of intracellular compartments) is required, we used an allele of *Vha100* (*V0a*) that specifically disrupts proton translocation (Kawasaki-Nishi et al., 2001; Williamson et al., 2010). Terminal cell expression of $Vha100^{R755A}$ resulted in defects identical to those caused by loss of V1 or V0, with both class 1 (55%) and class 2 (5%) observed (n=58; Fig. 3E,F). This established that acidification is required for maintenance of tube architecture.

Stalk cell autocellular tubes extend into *okg* and *cnj* terminal cells

Why do vATPase mutant terminal cells have long, branched autocellular tubes? Does this reflect a failure to switch from autocellular to seamless tubulogenesis, altered spatial regulation of where this switch occurs, or does the seamed tube come from the neighboring stalk cell, as occurs in wild-type fusion cells? The latter

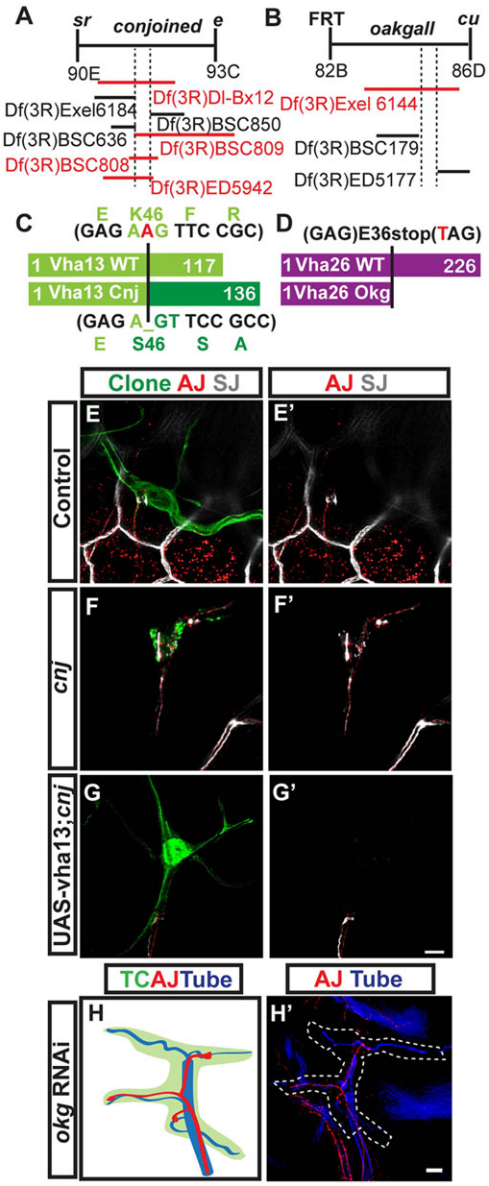

Fig. 2. *okg* and *cnj* encode subunits of the vATPase. Meiotic mapping of *okg* and *cnj*: *okg* between FRT^{82B} and *curled* (*cu*) (B), *cnj* between *stripe* (*sr*) and *ebony* (*e*) (A). Complementation tests with chromosomal deficiencies refined the map position. Sequence analysis identified single nucleotide changes (red) in *Vha26*/*okg* (D) introducing a STOP codon, and in *Vha13*/*cnj*, where the predicted frameshift encodes a larger, non-native protein (C, dark green). Deletions are indicated by red underscore. (E-G′) In mosaic experiments, a *Vha13* transgene restored wild-type connections and gas filling in *cnj* terminal cell clones: control (E,E′), *cnj* terminal cell (F,F′) and *cnj* terminal cell expressing UAS-Vha13 (G,G′) are shown; clone marker is *btl*>GFP (green), AJ (DE-cadherin, red), SJ (Fas3, white). (H,H′) SRF>*Vha26* RNAi (terminal cell, green) phenocopies *okg* EMS allele. Tube (blue) and AJ (red) are shown. Scale bars: 10 µm.

seemed likely, as seamed tubes within terminal cells appeared to terminate at internal intercellular junctions. However, the organization of seamed-to-seamless tube transitions remains unclear for terminal cells: some evidence suggests the connection of seamed and seamless tubes within a terminal cell ‘transition zone’ (Samakovlis et al., 1996; Song et al., 2013), whereas other data suggest that terminal cells make exclusively seamless tubes (Gervais and Casanova, 2010; Samakovlis et al., 1996; Song et al., 2013; Uv,

Development (2015) 142, 2048-2057 doi:10.1242/dev.119602

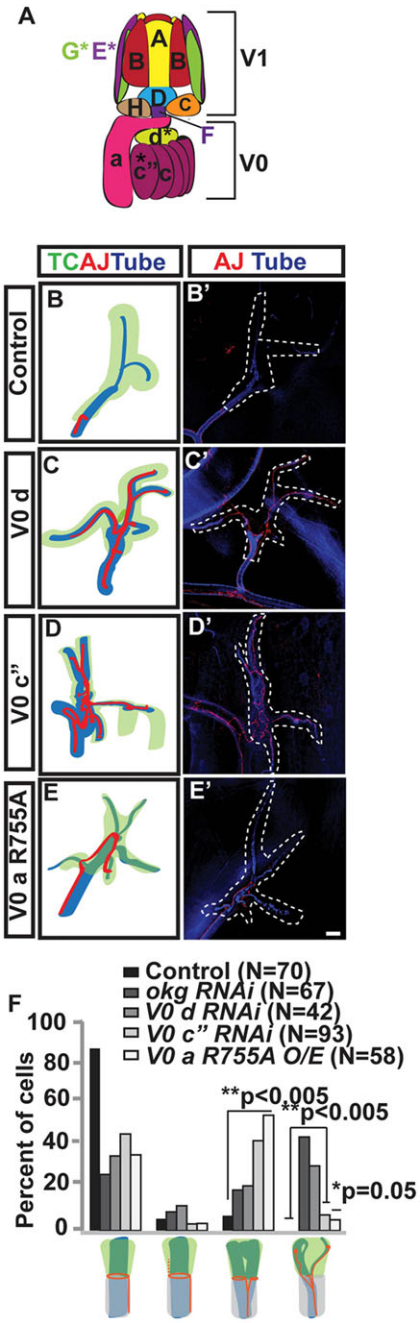

Fig. 3. Maintenance of the stalk cell-terminal cell interface requires vATPase holoenzyme function. (A) Okg (green) and Cnj (purple) heterodimers are part of the V1 domain (ATPase; subunits capitalized), and promote assembly/disassembly of the V1-V0 (membrane pore; lowercase) vATPase holoenzyme. (B-E′) *SRF*-GAL4 drives RNAi knockdown and/or GFP expression (terminal cell is outlined by the dashed white line): (B,B′) control, (C,C′) V0 d (both *VhaAC39-1* and *VhaAC39-2*) RNAi, (D,D′) *VhaPPA1-1*/ V0 c″ RNAi. (E,E′) *drm*-GAL4>V0 aR755A (pump-dead). (F) Quantification of phenotype frequency (see Fig. 1H for key). Scale bar: 10 µm.

2003). At wild-type stalk cell-fusion cell interfaces, the stalk cell extends a seamed tube into the fusion cell like “a finger poking into a balloon” (Uv, 2003) – note that these ‘fingers’ end in ring-like intercellular junctions; this has led to the suggestion that terminal cell autocellular tubes might also be stalk cell ‘fingers’. However, we and others see no evidence of this in wild-type terminal cells (Gervais and Casanova, 2010; Song et al., 2013).

To better understand terminal cell-stalk cell interfaces, we re-examined wild-type third instar larvae. We found that one cell membrane extends basolaterally from the intercellular AJ to ensheath a portion of the neighboring cell; a broad collar of intercellular SJ staining correlated with this area (supplementary material Fig. S2A,B,C). In some instances, terminal cells ensheathed stalk cells (supplementary material Fig. S2A,D), but stalk cells also ensheathed terminal cells (supplementary material Fig. S2B,E). Within 15% of terminal cells, we find a short, unbranched autocellular tube extending from the terminal cell seamless tube to the intercellular junction (Fig. 1H; supplementary material Fig. S1A,B) (Song et al., 2013), whereas 85% of terminal cells had only seamless tubes. Importantly, wild-type terminal cell autocellular tubes lack the internal ring-like structures that mark the distal ends of the stalk cell tube within fusion cells.

To test if seamed tubes in *okg* and *cnj* terminal cells belong to the stalk cell, we knocked down the SJ protein Fasciclin 3 (Fas3) exclusively in *cnj* terminal cells. If Fas3-positive seamed tubes were detected in *cnj, Fas3* RNAi terminal cells, then Fas3, and hence the tube, must belong to the stalk cell. As a control we depleted Fas3 from the stalk cell; we found that stalk cells were depleted for Fas3, but not other SJ or AJ proteins (supplementary material Fig. S3A,C). Knockdown in terminal cells was efficient, since control *Fas3* RNAi terminal cells lost their Fas3 collar staining (n=12; supplementary material Fig. S3D,E; Fig. 4A,B). In *cnj, Fas3* RNAi terminal cells, Fas3 was detected in seamed tubes running along the terminal cell, implying that the tubes belonged to the stalk cell (Fig. 4C).

As an independent test of seamed tube ownership, we utilized the Flybow system (Hadjieconomou et al., 2011) to differentially label neighboring stalk and terminal cells. In control larvae, terminal cell-stalk cell membranes were apposed at the site of initial cell-cell contact (Fig. 4D). In *okg* RNAi terminal cells, the autocellular tube was lined by stalk cell membrane that was partially or completely surrounded by terminal cell membrane (Fig. 4E,F). In some dramatic instances, terminal cell seamless tubes with no visible connection to each other were connected by stalk cell autocellular tube (Fig. 4F). These data suggested that *okg* and *cnj* apical membrane domains might be limiting, resulting in displacement of terminal cell seamless tubes distally, with compensatory branching and hypertrophy of stalk cell seamed tubes, the apical membrane domain of which is coupled to that of the terminal cell by AJs.

okg and *cnj* multicellular and autocellular tubes have reduced apical domains

If *okg* and *cnj* cells were unable to generate sufficient apical membrane, we hypothesized that it would compromise their ability to contribute to tubes of all architectures; therefore, we carefully tested *okg* and *cnj* dorsal trunk and stalk cell clones, which contribute to multicellular and autocellular tubes, respectively. In contrast to control dorsal trunk cells (Fig. 5A), *okg* and *cnj* dorsal trunk cells were not fully integrated into the epithelium and were oval, not hexagonal, in shape (Fig. 5B). Since the apical domain in epithelia lines the tube lumen, *okg* and *cnj* dorsal trunk clones had little or no apical domain. A statistically significant decrease in the ratio of apical membrane (area as defined by AJs) to cytoplasm (largest cross-sectional area as detected with cytoplasmic GFP) was observed in *cnj* dorsal trunk clones compared with control clones, which had a 1:1 ratio (Fig. 5C). In control autocellular tubes, stalk cells elongated along the long axis of the tube and connected to neighbors via ring-shaped intercellular junctions, with a single line of autocellular junctions running the length of the tube (Fig. 5D). By contrast, 89% (n=76) of *cnj* and 98% (n=95) of *okg* stalk cells did not have normal

Development (2015) 142, 2048-2057 doi:10.1242/dev.119602

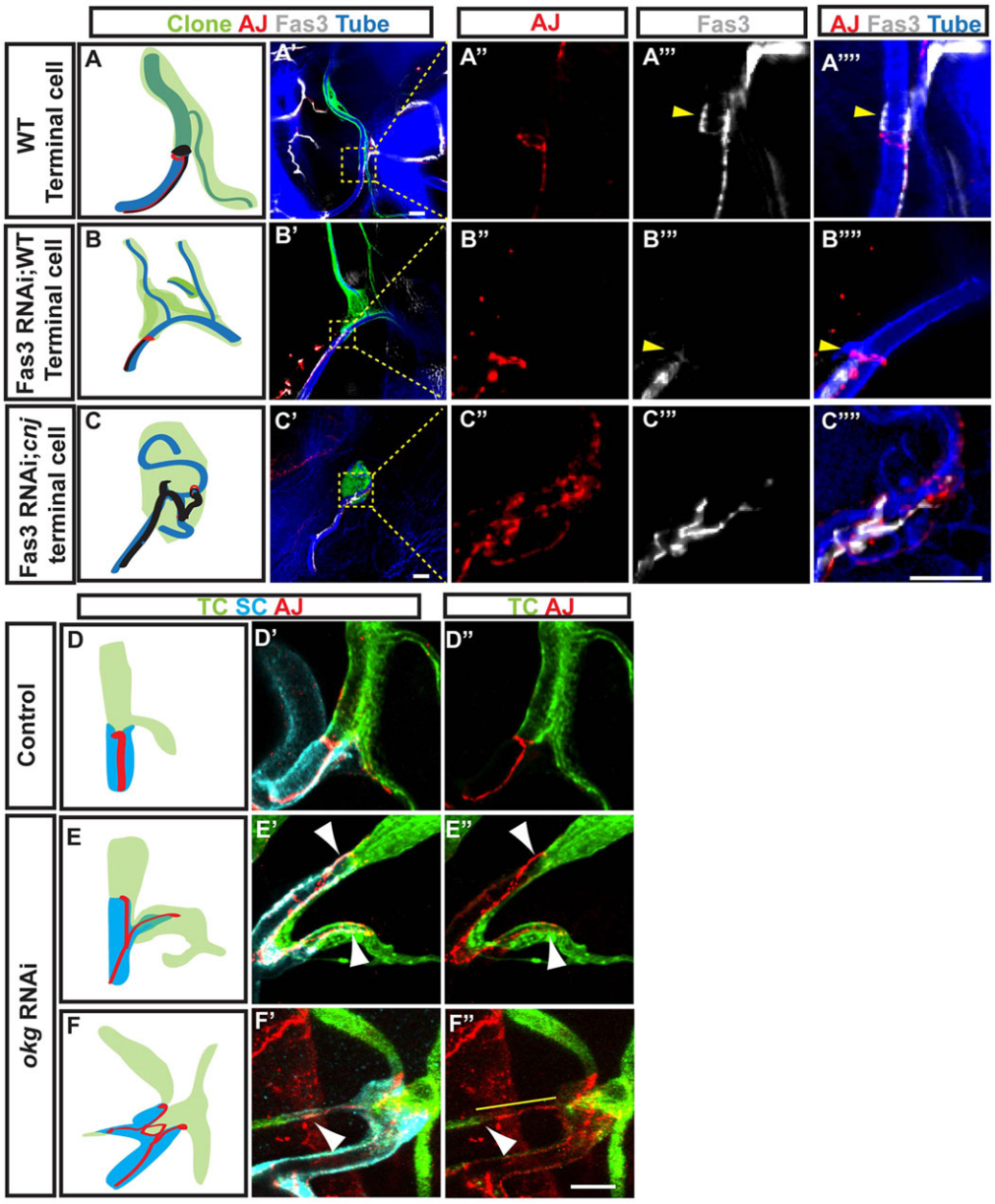

Fig. 4. Autocellular tubes in *okg* and *cnj* terminal cells belong to adjacent stalk cells. (A-C‴) To test whether autocellular tubes in mutant terminal cells are made by the terminal cell or neighboring stalk cell, Fas3 staining was assessed in terminal cell-specific *Fas3* RNAi. In control terminal cells (green) (A), a collar of SJ staining (gray) was detected (arrowhead); this staining was eliminated by *Fas3* RNAi (B). AJs (red) are also shown. (C) In *cnj, Fas3* RNAi clones, Fas3 staining was detected; thus, the neighboring stalk cell made and extended the seamed tube into the mutant terminal cell. (D-F″) Flybow-labeled terminal cell (green) and stalk cell (cyan) membranes, and AJs (red) were stained. (D) In controls, intercellular AJs decorated the initial contact between terminal cell and stalk cell membranes. In *okg* RNAi terminal cells (E,F), stalk cell membrane-surrounded tubes extended beyond the initial site of stalk cell-terminal cell contact (arrowhead). In an extreme case (F-F″), the stalk cell tube (yellow line) appeared to separate a terminal cell seamless tube from the terminal cell body. Scale bars: 10 µm.

autocellular or intercellular junctions (Fig. 5E); instead, these cells either detached from the epithelium or contributed a very short segment of autocellular tube, while the remaining cell cytoplasm bulged out of the tracheal epithelium (Fig. 5E′,E″). Interestingly, tubulogenesis is intact in *cnj* and *okg* embryos: we see no evidence of multicellular or autocellular tube defects in homozygous *cnj* embryos or in *cnj* stalk cell clones in first and second instar mosaic larvae, while dorsal trunk clones begin to round by second instar (supplementary material Fig. S1C,D,E,F-I). Thus, it is only over time, as the animal and its tracheal system increases dramatically in size, that tube architecture becomes disrupted.

Mutations in the Tor pathway phenocopy *okg* and *cnj*

Inhibition of the V-ATPase and Target of rapamycin (Tor) pathways have recently been reported to lead to reduced apical surface area (Gleixner et al., 2014). Thus, we sought to determine whether Tor-deficient terminal cells would phenocopy *okg* and *cnj*. Terminal cell-specific knockdown of Tor, expression of a dominant-negative Tor (Tor.TED) (Hennig and Neufeld, 2002), or knockdown of the Tor activator Rheb all lead to decreased terminal cell branching and a dramatic induction of class 2 defects [67% (n=26), 73% (n=24) and 48% (n=21), respectively] (Fig. 5F,G,H). These data are consistent with the Tor pathway acting through V-ATPase to expand the apical domain. Published data indicate that Tor regulates the expression of specific V-ATPase subunits (Gleixner et al., 2014) and, accordingly, we find that overexpression of Rheb, or of an activated form of the Tor downstream effector S6 kinase ($S6k^{SDTETE}$) (Barcelo and Stewart, 2002), does not suppress the *cnj* mutant terminal cell defects. These data imply that Tor acts genetically upstream of the V-ATPase (supplementary material Fig. S5) – although the pathway is more complex, as V-ATPase can also regulate mTOR (Jewell et al., 2013; Zoncu et al., 2011). Overall, these data support our hypothesis that limited apical membrane in *okg* and *cnj* cells leads to their displacement from the tube lumen by wild-type cells.

Apical proteins accumulate in intracellular puncta in *okg* and *cnj* terminal cells

Given that the V-ATPase and Tor pathways affect apical membrane surface area, we sought to determine whether apical

Development (2015) 142, 2048-2057 doi:10.1242/dev.119602

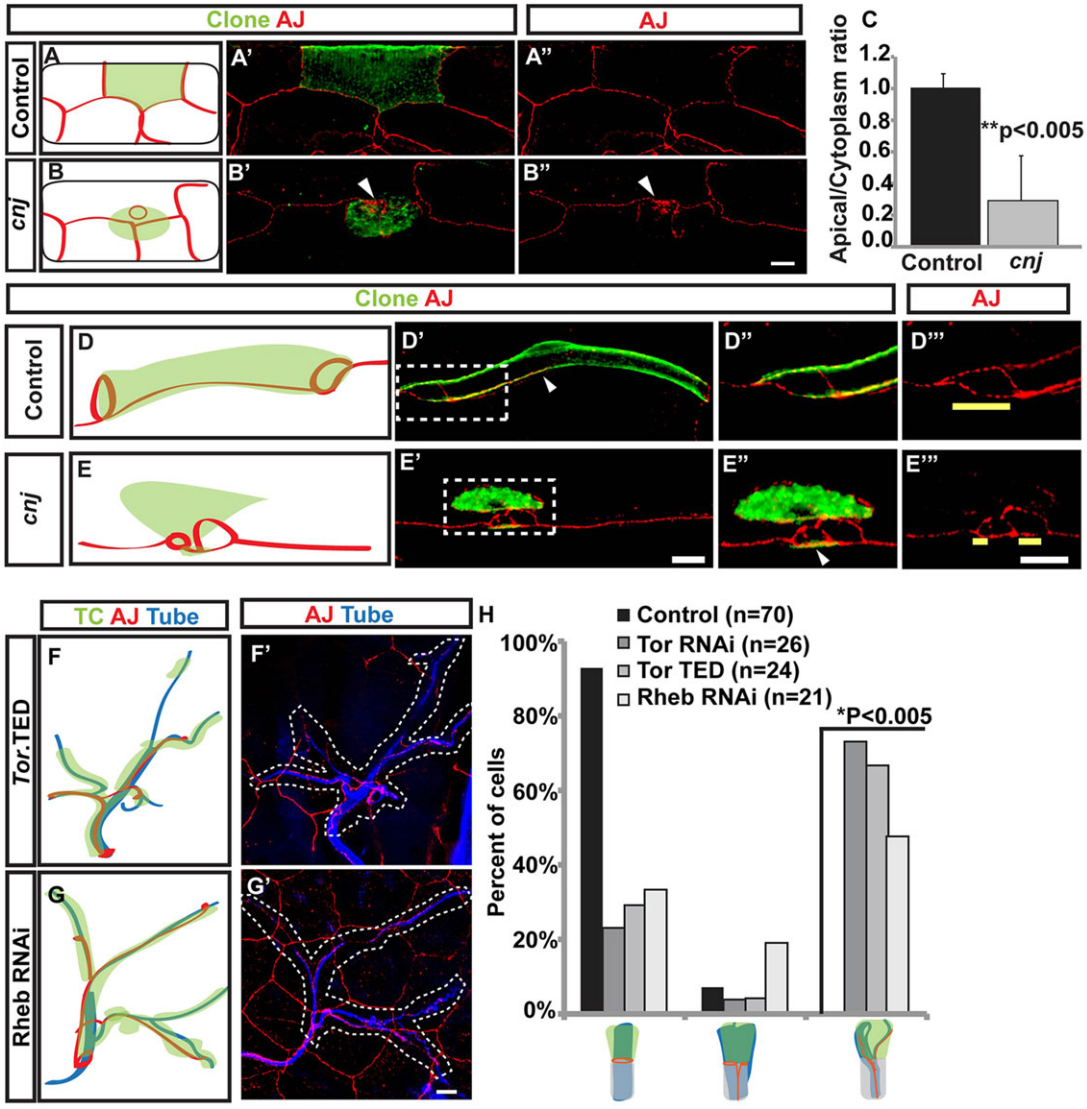

Fig. 5. Apical domain size and polarity are compromised in *okg* and *cnj*. In all tracheal cell types, *okg* and *cnj* clones (green) appeared to have undersized apical domains and to contribute little to tubes. (A-B″) In dorsal trunk clones, control cells (A) are hexagonal, make multiple intercellular AJs (red) and surround a portion of the lumen (A′,A″); by contrast, *cnj* dorsal trunk clones (B) appeared to be partially extruded from the epithelium, with diminished intercellular junction contacts (B′,B″, arrowhead). (C) Quantification of the reduction in the apical domain of *cnj* versus control cells. Error bars indicate s.d. (D-E‴) In control stalk cell clones, a line of staining (~80-90 µm, arrowhead) marks the autocellular tube seam (D′), with ring-like AJs marking intercellular junctions with proximal and distal stalk cells (D″, yellow line); by contrast, a *cnj* stalk cell (E,E′) is largely excluded from the epithelium, with only a short segment (<10 µm, arrowhead in E″) of autocellular tube connecting two intercellular junctions (yellow lines, E‴). (F-H) Tor pathway mutant terminal cells phenocopy loss of vATPase. (F-G′) Terminal cell (green) depletion of *Tor* and its activator *Rheb* in third instar larval filets is schematized (F,G) from micrographs (F′,G′), in which terminal cells are outlined. AJs (DE-cadherin, red) mark extended autocellular junctions along tubes (blue, UV) of *Tor*- and *Rheb*-depleted terminal cells. (H) Quantification of the frequency of junction phenotypes. Scale bars: 10 µm.

determinants were properly localized in vATPase- or Tor-deficient terminal cells. In wild type, Crumbs (Crb) localizes in foci at the terminal cell apical membrane (Fig. 6A) (Schottenfeld-Roames and Ghabrial, 2012); however, in vATPase-deficient cells, Crb levels were elevated but the steady-state localization was no longer to the lumenal membrane; rather, Crb was localized in large intracellular foci (Fig. 6B). We determined that aPKC, another apical polarity determinant (Wodarz et al., 2000), was similarly mislocalized in vATPase mutants (Fig. 6C,D). Likewise, we find that aPKC is mislocalized in Tor-DN and *Rheb* mutant terminal cells (Fig. 6E,F). Our results suggest that V-ATPase activity is required, downstream of Tor function, for localization of apical determinants.

To better understand how the transport of apical determinants is altered in the absence of V-ATPase function, we carried out extensive colocalization studies to determine which subcellular compartment(s) show an increased level of steady-state Crb. We found statistically significant changes in Crb colocalization with markers of the trans-Golgi (Galt) and early endosome (Rab5) (supplementary material Fig. S4A-K).

Cells deficient for apical determinants phenocopy *okg* and *cnj*

Another prediction of our model is that the loss of apical determinants alone should induce the stalk cell-terminal cell interface defects. We found that aPKC- or Par6-depleted terminal

Development (2015) 142, 2048-2057 doi:10.1242/dev.119602

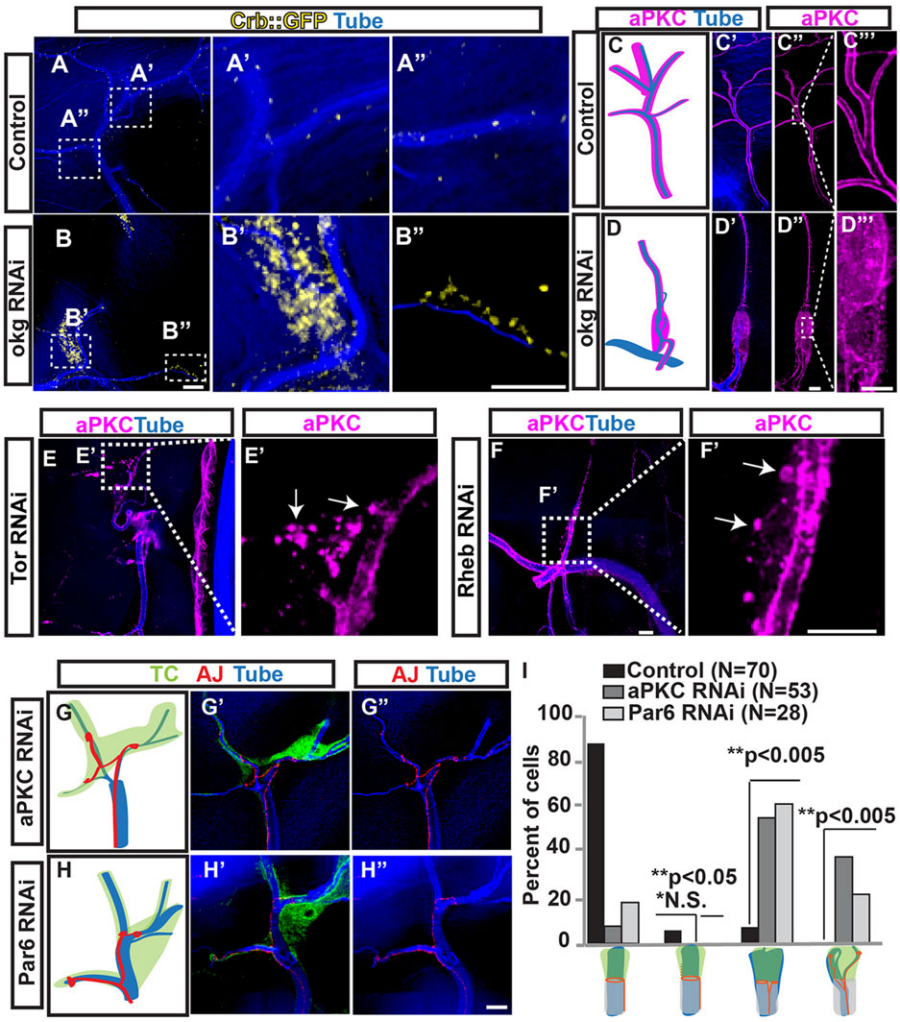

Fig. 6. Stalk cells respond to terminal cell apical polarity defects and injury. Apical polarity proteins are mislocalized in *okg*-depleted terminal cells. (A-D‴) Crumbs (Crb, yellow), aPKC (magenta) and tube (blue) staining are shown. In terminal cells, Crb and aPKC are apical in controls (A,C) and mislocalized in *okg*-depleted cells (B,D). In contrast to the small Crb foci detected in wild-type (A′,A″), large intracellular puncta of Crb are observed in *okg*-depleted terminal cells (B′,B″). aPKC marked the apical membrane of control terminal cells (C′-C‴), but was in large intracellular puncta in *okg* RNAi, *Tor* RNAi and *Rheb* RNAi terminal cells (D″,D‴,I,J). (E-F″) Knockdown of apical polarity proteins aPKC (G-G″) and Par6 (H-H″) conferred vATPase-like defects in tube organization. (I) Quantification of the frequency of junction phenotypes. Scale bars: 10 µm.

cells showed class 1 [55% (*n*=53) and 61% (*n*=28)] and class 2 [38% (*n*=53) and 21% (*n*=28)] defects (Fig. 6G,H,I). Thus, wild-type stalk cells compensate for terminal cells with reduced apical domains by hypertrophy and branching of their autocellular tubes.

Physiological induction of the stalk cell compensatory branching response

We found that genetic reduction of the terminal cell apical membrane elicited a novel compensatory response in the neighboring stalk cell, and because we also noted the presence of class 1 defects at low incidence in wild type (4%, *n*=84), we next asked if the response could be physiologically induced. We found that in a pinch wound assay, in which second and early third instar control larvae were injured with forceps, within 24-48 h 27% (*n*=117) of injured terminal cells had class 1 defects and an additional 24% (*n*=117) had class 2 defects (Fig. 7A,B).

Next, we sought to determine whether a connection exists between terminal cell injury and maintenance of the apical domain. Injury to Crb-depleted (RNAi) terminal cells, which normally do not display junction defects, increased the frequency of class 2 defects (Fig. 7C). These data suggest that cells with a compromised ability to generate new apical membrane are sensitized for invasion by the stalk cell. Interestingly, we find that at least some aspects of the wound-healing response are induced by both genetic and physiological perturbations of terminal cells. In the larval epidermis, cells adjacent to a wound activate Jun kinase, leading to expression of *puckered* (*puc*), a negative-feedback component of the pathway (Galko and Krasnow, 2004). We observed increased *puc-lacZ* expression in stalk cells that displayed compensatory branching near injured terminal cells or near genetically comprised terminal cells (Fig. 7D). Taken together, these data suggest that the wounding-induced and the genetically induced compensatory stalk cell branching responses intersect.

DISCUSSION

Our data, together with previous indications in the literature, draw a strong connection between vATPase function, apical proteins and apical surface area. In some epithelia, vATPase itself is apical (Hurtado-Lorenzo et al., 2006; Liegeois, 2006), and Kanda et al. (2013) established a direct interaction between Atp6ap2, an accessory subunit of the vATPase, and the Par3 polarity protein in mice; furthermore, tissue-specific *Atp6ap2* knockout mice displayed severe retinal polarity defects. Recent work from the Simons laboratory (Gleixner et al., 2014) suggests that vATPase function, together with mTOR signaling, is essential for apical endocytosis and apical surface area growth. Our results in a distinct epithelium are consistent with a role of vATPase in the regulation of apical surface area. The Gleixner et al. study demonstrated a defect in apical endocytosis in V-ATPase mutant wing disc epithelia, with uptake of dextrans and avidin compromised by downregulation of Megalin and decreased apical surface area (Gleixner et al., 2014). Our studies

Development (2015) 142, 2048-2057 doi:10.1242/dev.119602

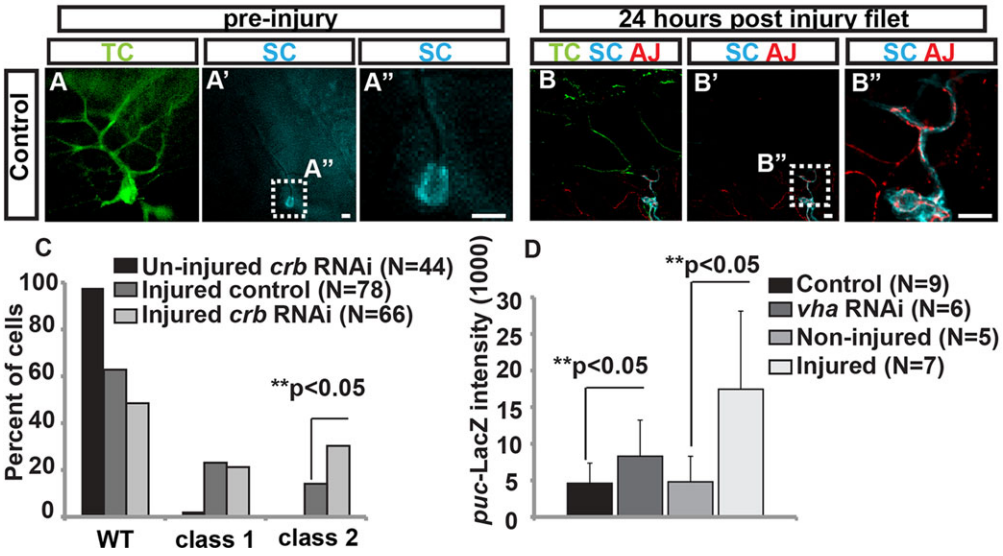

Fig. 7. Stalk cells branch in response to physiological injury. (A) Pre-injury, a terminal cell (green) connected to an unbranched stalk cell (cyan; A′,A‴) is shown. (B) A pinch injury to the cell shown in A induces stalk cell branching (B′,B″). Autocellular tubes (DE-cadherin, red) are associated with the responding stalk cell branches outlined in B″ and at the wounded terminal-healthy stalk cell interface (B′,B″). (C) Terminal cells depleted of Crb by RNAi are sensitized to injury and show an increased frequency of class 2 defects. (D) Stalk cell branching adjacent to injured and VhaPPA1-1-depleted terminal cells induced *puc* expression. Pixel intensity is quantified in D. Error bars indicate s.d. Scale bars: 10 µm.

indicate that, in addition to affecting apical endocytosis, V-ATPase deficiency alters other transport pathways that are crucial for the regulation of apical surface area. Indeed, disruption of endocytosis specifically in the tracheal epithelium results in increased apical membrane surface area (Schottenfeld-Roames et al., 2014), whereas loss of V-ATPase function results in a reduction in apical surface area. In V-ATPase-deficient terminal cells we see an aberrant accumulation of Crb within the trans-Golgi, as well as within early endosomes. This suggests that there is a defect in the delivery of Crb to the apical membrane, as well as a defect in the delivery of endocytosed Crb to the lysosomal compartment. Indeed, although the lysosomal compartment appears dramatically enlarged in V-ATPase mutant cells – presumably owing to inefficient turnover of proteins, as V-ATPase function is required to acidify the lysosome – we could detect no significant increase of Crb within the lysosome. Thus, our data support a requirement for V-ATPase downstream of mTOR for the proper targeting of apical determinants to the plasma membrane.

Our results also point to a novel mechanism of compensatory tube branching. During larval life, branching morphogenesis was thought to be the exclusive purview of seamless tubes formed by terminal cells. Terminal cells are induced to branch by hypoxia, and normally tile on target tissues. However, terminal cells defective in gas transport permit the compensatory growth of neighboring terminal cells into undersupplied areas (Centanin et al., 2008; Jarecki et al., 1999). Our data uncover an unappreciated ability of autocellular tube-forming stalk cells to undergo ectopic growth and branching to compensate for terminal cells that are unable to sufficiently expand their apical membrane owing to genetic defect or injury. Stalk cell compensatory branching occurs prior to the re-entry of dorsal branch stalk cells into the cell cycle – a process that remodels the larval tracheal system during puparium formation (Weaver and Krasnow, 2008); it also occurs in more posterior dorsal branches, in which stalk cells are never observed to behave as facultative stem cells.

MATERIALS AND METHODS

Fly strains

The following fly strains were used: *Vha26*^{GD7112} (*okg*) RNAi, *VhaPPA1-1*^{GD16478} (*V0 c″*) RNAi, *VhaAC39-1*^{GD9859}; *VhaAC39-2*^{GD10714} (V0 d), FasIII RNAi^{GD80}, *aPKC*^{JF01966} RNAi, *Par6* RNAi^{HMS01829}, *Rheb* RNAi^{HMS00923}, UAS-*Tor*.TED, *Tor* RNAi^{HMS01114}, UAS-S6k^{SDTETE}, UAS-GFP:Sec15, UAS-golgi:RFP, UAS-Kdel:RFP, UAS-Rab5:YFP, *puc*$^{A251.1}$ *lacZ* (Bloomington), *Vha44*^{KG00951} FRT^{42D}/CyO and *Vha68-2* FRT^{40A}/CyO (DGRC, Kyoto, Japan), *Vha55*^{i2E9}/TM3 (Bloomington) recombined onto an FRT by D.F., Crb::GFP [gift of Y. Hong (Huang et al., 2011)], UAS-Lamp1:GFP (gift of H. Kramer, University of Texas Southwestern, Dallas, USA), *SRF*-GAL4 (gift of M. Metzstein, University of Utah, Salt Lake City, USA), *btl*-GAL4 and *drm*-GAL4 (Bloomington). EMS alleles of *okg* and *cnj* were generated previously (Ghabrial et al., 2011). *P* element failing to complement *okg*^{696}: P{lacW}*noi*^{i3E7} *Vha26*^{i3E7}/TM3, P{ftz/lacZ}SC1, ry^{RK} Sb^{1} Ser^{1}. *P* element failing to complement *cnj*^{356}: P{PTT-GA}*Vha13*^{CA07644}/TM3. Df(3R) Exel6144 uncovered *okg*^{696} and Df(3R)BSC805 uncovered *cnj*^{356} (Bloomington).

Tissue-specific RNAi and misexpression experiments

SRF-GAL4 drove expression of UAS-GFP and *Vha26*^{GD7112} (*okg*) RNAi, *VhaPPA1-1*^{GD16478} (*V0 c″*) RNAi, *VhaAC39-1*^{GD9859}; *VhaAC39-2*^{GD10714} (V0 d), *Par6* RNAi^{HMS01829} RNAi and *aPKC*^{JF01966} RNAi, *Rheb*^{HMS00923} RNAi, UAS-Tor.TED, *Tor*^{HMS01114} RNAi at 29°C. *drm*-GAL4 drove expression of UAS-GFP and V0a R755A at 22°C.

Temperature shift experiments

The following crosses were used: *Tub*-GAL80^{ts}; *Vha26*^{GD7112}/TM6B *Tb* crossed to *Sp*/CyO; *SRF*-GAL4, UAS-CD8::GFP/TM3. Embryos were collected for 8 h and maintained at 18°C until upshift to 29°C. Larvae were collected for immunostaining at third instar.

Rescue construct

Generation of UASt-*Vha13*: *Vha13* complementary DNA AT14009 (DGRC) was digested (*Xho*I and *Eco*RI) and ligated into pUAST (Brand and Perrimon, 1993). The transgene was injected into *w*^{1118} embryos to generate UAS-*Vha13* transgenic flies (Bestgene).

Determining seamed tube origin

FasIII RNAi^{GD80}, FRT^{82B}+(or FRT^{82B} *cnj*) were crossed to *btl*-GAL4, UAS-GFP; FRT^{82B} *Tub*-GAL80 to generate MARCM clones (Lee and Luo, 2001).

Flybow experiments

The following crosses were used: *SRF*-GAL4; hs-mFLP5 was crossed to UAS-flybow1.1; UAS-*Vha26*^{GD7112}. Developing embryos and larvae were heat shocked three times and kept at 25°C until they were collected at third larval instar. Images were collected on a Zeiss 510 Meta confocal microscope and processed using Fiji (ImageJ) and Photoshop (Adobe) software.

Colocalization experiments

The following crosses were used: FRT^{82B} *cnj* flies were crossed to UAS-Rab5:YFP, UAS-GFP:Sec15, UAS-golgi:RFP, UAS-Kdel:RFP or

Development (2015) 142, 2048-2057 doi:10.1242/dev.119602

UAS-Lamp1:GFP. Mosaic larvae were filleted and stained with anti-GFP, anti-RFP and anti-Crb antibodies (as described below). Images were collected on the Zeiss 510 Meta confocal microscope and processed using Fiji [Pearson's colocalization coefficient (*r*) was determined using the Coloc2 plug-in] and Photoshop software.

Sequence analyses

okg genomic DNA, *cnj* genomic DNA and control genomic DNA from the parental strain on which *okg* and *cnj* mutations were induced were amplified by PCR and sequenced. Primer pairs are described in supplementary material Table S1.

Transgene rescue of *cnj* terminal cells

The following crosses were carried out: UAS-Vha13; FRT^{82B} *cnj*^{356}/TM6B flies were crossed to *btl*-GAL4, UAS-GFP/CyO; FRT^{82B} *Tub*-GAL80/TM6B. Mosaic larvae with GFP-marked clones were collected for immunostaining.

Immunohistochemistry

Third instar larvae were filleted, fixed in 4% paraformaldehyde (EMS) and washed in 1× PBS containing 0.3% Tween 20 and 0.3% Triton X-100. The following antibodies were used: rat anti-DE-cadherin (DCAD2; 1:20; DSHB), rabbit anti-Wkd peptide (1:750) (Schottenfeld-Roames and Ghabrial, 2012), chicken anti-GFP (1:1000; Invitrogen, A10262), mouse anti-Fas3 (1:50; DSHB), mouse anti-Armadillo (1:200; DSHB), mouse anti-RFP (1:1000; Abcam, 65866), rabbit anti-Varicose (1:500; gift of E. Knust, Max Plank Institute of Molecular Cell Biology and Genetics, Dresden, Germany), rat anti-Crb (1:100; gift of E. Knust) and rabbit anti-PKCzeta (aPKC; 1:200; Santa Cruz, sc-216). Alexa Fluor-conjugated secondary antibodies were goat anti-chicken 488, goat anti-mouse 555, donkey anti-rat 647 and goat anti-rat 555 (Invitrogen). Larvae were mounted in Aqua Polymount (Polysciences) and images were acquired on Leica DM5500 and DMI6000 B microscopes. *z*-stacks were captured and processed with Leica and Fiji software. Projected *z*-stacks are shown, unless noted otherwise. Statistical significance was determined using Fisher's exact probability test and/or Student's *t*-test (www.vasserstats.net).

puc-lacZ intensity

The following crosses were used: UAS-VhaPPA1-1/+, *puc-lacZ* males were crossed to SRF>GFP at 29°C. VhaPPA1-1; *puc-lacZ*/SRF>GFP and sibling controls with *puc-lacZ* and SRF>GFP alone were collected. Third instar SRF>GFP/*puc-lacZ* larvae were subjected to a pinch assay as described below. All collected larvae were immunostained and images were captured on the Leica DMI6000 B microscope. Exposure and intensity were kept constant. The corrected total cell fluorescence (CTCF) was measured as previously described Burgess et al., 2010. Statistical significance was determined using Student's *t*-test (www.vasserstats.net).

Quantifying the ratio of apical to cytoplasmic area

The cytoplasm (GFP) and apical domain (DE-cadherin) of control and *cnj* dorsal trunk cells were outlined and the area measured using Fiji. Standard deviation and statistical significance (Student's *t*-test) were determined (Excel).

Mapping the mutations in *okg* and *cnj*

Meiotic recombination placed *okg* and *cnj* between FRT^{82B} and the visible recessive marker *curled* (*cu*), or the visible recessive markers *striped* (*sr*) and *ebony* (*e*), respectively. Complementation tests against deficiency strains spanning the interval between the FRT and *cu* revealed that *okg* was uncovered by Df(3R)Exel6144, which deletes the segment of the chromosome between 83A6 to 83B6. Mutants within this region were tested against *okg*^{696} for complementation.

Pinch assay

For double-labeled membranes: *yw* hsFLP122; *btl*>Gal4; FRT^{82B} UAS-Td Tomato females were crossed to *btl*>Gal4; FRT^{82B} UAS-myrGFP males and heat shocked for 1 h to induce either green, red or yellow tracheal cells. Quantification was performed on larvae from the yw FLP122, *btl*>Gal4, UAS-GFP or UAS-RFP; FRT^{2A}, FRT^{82B}, SRF>GFP; SRF>GFP, UAS-*crb* RNAi and SRF>GFP/*puc-lacZ* strains. Late second and third instar larvae were identified based on spiracles and size. Larvae were pinched with forceps under the dissecting microscope. Disruption of terminal cell gas filling was used to monitor terminal cell injury. Larvae were incubated at room temperature and collected 24 h post injury for filet and immunostaining.

Epistasis experiments

The following crosses were used: UAS-Rheb.Pa, FRT^{82B} *cnj*/TM6b and UAS-S6k SDTETE/UAS-TwdlD::Mkate; FRT^{82B} *cnj*/TM6b males were crossed to *btl*>mCD8GFP; FRT^{82B} GFP RNAi virgins. Third instar larvae with clones were grown at 29°C, filleted and immunostained for clone markers and AJs as described.

Acknowledgements

We thank E. Knust, P. Rorth, N. Harden, G. Miesenboek, R. Hiesinger and M. Simons for reagents; the CDB Microscopy Core for assistance; S. DiNardo, M. Sundaram and the A.S.G. and DiNardo laboratories for discussions and comments on the manuscript.

Competing interests

The authors declare no competing or financial interests.

Author contributions

D.F. and A.S.G. conceived the experiments, D.F. carried them out, and D.F. and A.S.G. interpreted the data and wrote the manuscript.

Funding

A.S.G. thanks the University of Pennsylvania and the National Institutes of Health (NIH) [1R01GM089782] for funding. D.F. acknowledges an NIH training grant [T32HD007516]. This work was supported in part by a Basil O'Connor Starter Scholar Research Award [grant no. 5-FY09-43] from the March of Dimes Foundation. Deposited in PMC for release after 12 months.

Supplementary material

Supplementary material available online at
http://dev.biologists.org/lookup/suppl/doi:10.1242/dev.119602/-/DC1

References

Andrew, D. J. and Ewald, A. J. (2010). Morphogenesis of epithelial tubes: insights into tube formation, elongation, and elaboration. *Dev. Biol.* **341**, 34-55.

Barcelo, H. and Stewart, M. J. (2002). Altering Drosophila S6 kinase activity is consistent with a role for S6 kinase in growth. *Genesis* **34**, 83-85.

Bayer, M. J., Reese, C., Buhler, S., Peters, C. and Mayer, A. (2003). Vacuole membrane fusion: V0 functions after trans-SNARE pairing and is coupled to the Ca^{2+}-releasing channel. *J. Cell Biol.* **162**, 211-222.

Blum, Y., Belting, H.-G., Ellertsdottir, E., Herwig, L., Lüders, F. and Affolter, M. (2008). Complex cell rearrangements during intersegmental vessel sprouting and vessel fusion in the zebrafish embryo. *Dev. Biol.* **316**, 312-322.

Brand, A. H. and Perrimon, N. (1993). Targeted gene expression as a means of altering cell fates and generating dominant phenotypes. *Development* **118**, 401-415.

Burgess, A., Vigneron, S., Brioudes, E., Labbé, J.-C., Lorca, T. and Castro, A. (2010). Loss of human Greatwall results in G2 arrest and multiple mitotic defects due to deregulation of the cyclin B-Cdc2/PP2A balance. *Proc. Natl. Acad. Sci. USA 107*, 12564-12569.

Centanin, L., Dekanty, A., Romero, N., Irisarri, M., Gorr, T. A. and Wappner, P. (2008). Cell autonomy of HIF effects in Drosophila: tracheal cells sense hypoxia and induce terminal branch sprouting. *Dev. Cell* **14**, 547-558.

Di Giovanni, J., Boudkkazi, S., Mochida, S., Bialowas, A., Samari, N., Lévêque, C., Youssouf, F., Brechet, A., Iborra, C., Maulet, Y. et al. (2010). V-ATPase membrane sector associates with synaptobrevin to modulate neurotransmitter release. *Neuron* **67**, 268-279.

Doherty, R. D. and Kane, P. M. (1993). Partial assembly of the yeast vacuolar H (+)-ATPase in mutants lacking one subunit of the enzyme. *J. Biol. Chem.* **268**, 16845-16851.

Galko, M. J. and Krasnow, M. A. (2004). Cellular and genetic analysis of wound healing in Drosophila larvae. *PLoS Biol.* **2**, E239.

Gervais, L. and Casanova, J. (2010). In vivo coupling of cell elongation and lumen formation in a single cell. *Curr. Biol.* **20**, 359-366.

Gervais, L., Lebreton, G. and Casanova, J. (2012). The making of a fusion branch in the Drosophila trachea. *Dev. Biol.* **362**, 187-193.

Ghabrial, A., Luschnig, S., Metzstein, M. M. and Krasnow, M. A. (2003). Branching morphogenesis of the Drosophila tracheal system. *Annu. Rev. Cell Dev. Biol.* **19**, 623-647.

Ghabrial, A. S., Levi, B. P. and Krasnow, M. A. (2011). A systematic screen for tube morphogenesis and branching genes in the Drosophila tracheal system. *PLoS Genet.* **7**, e1002087.
Gleixner, E. M., Canaud, G., Hermle, T., Guida, M. C., Kretz, O., Helmstädter, M., Huber, T. B., Eimer, S., Terzi, F. and Simons, M. (2014). V-ATPase/mTOR signaling regulates megalin-mediated apical endocytosis. *Cell Rep.* **8**, 10-19.
Hadjieconomou, D., Rotkopf, S., Alexandre, C., Bell, D. M., Dickson, B. J. and Salecker, I. (2011). Flybow: genetic multicolor cell labeling for neural circuit analysis in Drosophila melanogaster. *Nat. Methods* **8**, 260-266.
Hennig, K. M. and Neufeld, T. P. (2002). Inhibition of cellular growth and proliferation by dTOR overexpression in Drosophila. *Genesis* **34**, 107-110.
Herwig, L., Blum, Y., Krudewig, A., Ellertsdottir, E., Lenard, A., Belting, H.-G. and Affolter, M. (2011). Distinct cellular mechanisms of blood vessel fusion in the zebrafish embryo. *Curr. Biol.* **21**, 1942-1948.
Hiesinger, P. R., Fayyazuddin, A., Mehta, S. Q., Rosenmund, T., Schulze, K. L., Zhai, R. G., Verstreken, P., Cao, Y., Zhou, Y., Kunz, J. et al. (2005). The v-ATPase V0 subunit a1 is required for a late step in synaptic vesicle exocytosis in Drosophila. *Cell* **121**, 607-620.
Hildenbrand, Z. L., Molugu, S. K., Stock, D. and Bernal, R. A. (2010). The C-H peripheral stalk base: a novel component in V1-ATPase assembly. *PLoS ONE* **5**, e12588.
Huang, J., Huang, L., Chen, Y.-J., Austin, E., Devor, C. E., Roegiers, F. and Hong, Y. (2011). Differential regulation of adherens junction dynamics during apical-basal polarization. *J. Cell Sci.* **124**, 4001-4013.
Hurtado-Lorenzo, A., Skinner, M., El Annan, J., Futai, M., Sun-Wada, G.-H., Bourgoin, S., Casanova, J., Wildeman, A., Bechoua, S., Ausiello, D. A. et al. (2006). V-ATPase interacts with ARNO and Arf6 in early endosomes and regulates the protein degradative pathway. *Nat. Cell Biol.* **8**, 124-136.
Isaac, D. D. and Andrew, D. J. (1996). Tubulogenesis in Drosophila: a requirement for the trachealess gene product. *Genes Dev.* **10**, 103-117.
Jarecki, J., Johnson, E. and Krasnow, M. A. (1999). Oxygen regulation of airway branching in Drosophila is mediated by branchless FGF. *Cell* **99**, 211-220.
Jewell, J. L., Russell, R. C. and Guan, K. L. (2013). Amino acid signalling upstream of mTOR. *Nat. Rev. Mol. Cell Biol.* **14**, 133-139.
Kanda, A., Noda, K., Yuki, K., Ozawa, Y., Furukawa, T., Ichihara, A. and Ishida, S. (2013). Atp6ap2/(pro)renin receptor interacts with Par3 as a cell polarity determinant required for laminar formation during retinal development in mice. *J. Neurosci.* **33**, 19341-19351.
Kawasaki-Nishi, S., Nishi, T. and Forgac, M. (2001). Arg-735 of the 100-kDa subunit a of the yeast V-ATPase is essential for proton translocation. *Proc. Natl. Acad. Sci. USA* **98**, 12397-12402.
Lee, T. and Luo, L. (2001). Mosaic analysis with a repressible cell marker (MARCM) for Drosophila neural development. *Trends Neurosci.* **24**, 251-254.
Liegeois, S. (2006). The V0-ATPase mediates apical secretion of exosomes containing Hedgehog-related proteins in Caenorhabditis elegans. *J. Cell Biol.* **173**, 949-961.
Lin, M., Li, S. C., Kane, P. M. and Höfken, T. (2012). Regulation of vacuolar H+-ATPase activity by the Cdc42 effector Ste20 in Saccharomyces cerevisiae. *Eukaryot. Cell* **11**, 442-451.
Ohira, M., Smardon, A. M., Charsky, C. M. H., Liu, J., Tarsio, M. and Kane, P. M. (2006). The E and G subunits of the yeast V-ATPase interact tightly and are both present at more than one copy per V1 complex. *J. Biol. Chem.* **281**, 22752-22760.
Okamoto-Terry, H., Umeki, K., Nakanishi-Matsui, M. and Futai, M. (2013). Glu44 in the amino-terminal α-helix of yeast vacuolar ATPase E subunit (Vma4p) has a role for VoV1 assembly. *J. Biol. Chem.* **288**, 36236-36243.
Samakovlis, C., Hacohen, N., Manning, G., Sutherland, D. C., Guillemin, K. and Krasnow, M. A. (1996). Development of the Drosophila tracheal system occurs by a series of morphologically distinct but genetically coupled branching events. *Development* **122**, 1395-1407.
Schottenfeld-Roames, J. and Ghabrial, A. S. (2012). Whacked and Rab35 polarize dynein-motor-complex-dependent seamless tube growth. *Nat. Cell Biol.* **14**, 386-393.
Schottenfeld-Roames, J., Rosa, J. B. and Ghabrial, A. S. (2014). Seamless tube shape is constrained by endocytosis-dependent regulation of active moesin. *Curr. Biol.* **24**, 1756-1764.
Smardon, A. M., Tarsio, M. and Kane, P. M. (2002). The RAVE complex is essential for stable assembly of the yeast V-ATPase. *J. Biol. Chem.* **277**, 13831-13839.
Song, Y., Eng, M. and Ghabrial, A. S. (2013). Focal defects in single-celled tubes mutant for Cerebral cavernous malformation 3, GCKIII, or NSF2. *Dev. Cell* **25**, 507-519.
Strasser, B., Iwaszkiewicz, J., Michielin, O. and Mayer, A. (2011). The V-ATPase proteolipid cylinder promotes the lipid-mixing stage of SNARE-dependent fusion of yeast vacuoles. *EMBO J.* **30**, 4126-4141.
Strilić, B., Kučera, T. and Lammert, E. (2010). Formation of cardiovascular tubes in invertebrates and vertebrates. *Cell. Mol. Life Sci.* **67**, 3209-3218.
Tomashek, J. J., Graham, L. A., Hutchins, M. U., Stevens, T. H. and Klionsky, D. J. (1997). V1-situated stalk subunits of the yeast vacuolar proton-translocating ATPase. *J. Biol. Chem.* **272**, 26787-26793.
Uv, A. (2003). Drosophila tracheal morphogenesis: intricate cellular solutions to basic plumbing problems. *Trends Cell Biol.* **13**, 301-309.
Weaver, M. and Krasnow, M. A. (2008). Dual origin of tissue-specific progenitor cells in Drosophila tracheal remodeling. *Science* **321**, 1496-1499.
Williamson, W. R., Wang, D., Haberman, A. S. and Hiesinger, P. R. (2010). A dual function of V0-ATPase a1 provides an endolysosomal degradation mechanism in Drosophila melanogaster photoreceptors. *J. Cell Biol.* **189**, 885-899.
Wodarz, A., Hinz, U., Engelbert, M. and Knust, E. (1995). Expression of crumbs confers apical character on plasma membrane domains of ectodermal epithelia of Drosophila. *Cell* **82**, 67-76.
Wodarz, A., Ramrath, A., Grimm, A. and Knust, E. (2000). Drosophila atypical protein kinase C associates with Bazooka and controls polarity of epithelia and neuroblasts. *J. Cell Biol.* **150**, 1361-1374.
Wolff, J. R. and Bär, T. (1972). 'Seamless' endothelia in brain capillaries during development of the rat's cerebral cortex. *Brain Res.* **41**, 17-24.
Zoncu, R., Bar-Peled, L., Efeyan, A., Wang, S., Sancak, Y. and Sabatini, D. M. (2011). mTORC1 senses lysosomal amino acids through an inside-out mechanism that requires the vacuolar H(+)-ATPase. *Science* **334**, 678-683.